https://dx.doi.org/10.4314/dujopas.v10i2c.16
ISSN (Print): 2476-8316
ISSN (Online): 2635-3490
Dutse Journal of Pure and Applied Sciences (DUJOPAS), *Vol. 10 No. 2c June 2024*

Density Functional Theory Study of the Nuclear Magnetic Resonance Properties and Natural Bond Orbital Analysis of Germanium-Phenyl Nanocluster

Njapba S. Augustine[1] and Galadanci M. S. Garba[2]
[1]Department of Physics,
Gombe State University,
PMB 127,
Gombe State,
Nigeria.

[2]Department of Physics,
Bayero University,
Kano PMB 3011,
Kano State,
Nigeria.

Abstract

In this study, the optimized molecular geometry and vibrational frequencies of novel germanium-phenyl nanostructure were calculated using the hybrid functional B3LYP/Lanl2dz as implemented in Gaussian 09 program. The obtained geometries from the calculations of density functional theory were used to carry out natural bond orbital analysis. The stabilization energy E_2 that is related to the delocalization trend of electrons from donor to acceptor orbitals was also computed. The higher the stabilization energy E_2, between a bonding orbital and an acceptor orbital the greater the interaction between them, signifying clear evidence of stabilization that is originating from the hyperconjugation of H-bonded interaction. Our results reveal strong stabilization energy E_2, of orbital interaction between the bonding orbitals (Ge_4-Ge_6) and non-lone pair Ge_8 with value of 81.36 Kcal/mol. The NMR isotropic chemical shift and magnetic shielding of [$Ge_9(C_6H_5)$] nanostructure were calculated using Gauge-including atomic orbitals(GIAO) algorithm and results compared with experimental data. The theoretically calculated values of the coupling constant in the gas phase are $^3J(H-H)=10.99$ Hz, $^3J(C-H)=10.99$ Hz, and $^3J(C-C)=12.99$ Hz respectively and are observed to be bigger than the experimental value with a difference of about 3.29 Hz. The spin-spin coupling constant ^3J was calculated by means of the generalized Karplus-type relationship.

Keywords: DFT, stabilization energy, magnetic shielding, chemical shift, Natural bond orbital.

INTRODUCTION

Materials are important for the development and technological growth of any society. How far any society has advanced technologically is a good indication of its advancement in material science and technology. Our lives have been made so comfortable today as a result of availability of materials and devices made thereof. One such material that has emerged of recent because of its superior properties for use in modern technology and smart devices is the organic-inorganic hybrid nanostructure materials. Hybrids have demonstrated better

Author for Correspondence

material properties when integrated as device components compared to its individual inorganic counterparts (Kagan *et al*., 1999; Carroro and Gross, 2014). This new material is sought for improved optical and electrical properties, luminescence, ionic conductivity and selectivity as well as chemical or biochemical activity (Mir, 2018). Hybrid organic-inorganic crystalline materials have characteristic features that combine the highly optical nonlinear and chemical flexibility of organic materials with the physical ruggedness of the inorganics on a molecular scale with tremendous number of materials (Abbas *et al*, 2019). Organic molecules show extremely large nonlinear optical response through the high polarizability of π-conjugated molecules. This allows charge transfer within the molecule as a response to the external electric field. Other factors also that contribute to nonlinear response in these molecules are the planarity of the molecules, molecular symmetry and dimensionality of charge transfer networks. The inorganic elements cover most of the periodic table, often need high-tech and high power equipment to be processed. However, their robust and high performance electric and magnetic properties are unequalled and therefore the inorganic materials are extensively used in conventional electronics. Organic-inorganic hybrid functional materials are being utilized in many diverse areas including optics, micro-electronics, transportation, health, energy, energy storage, diagnosis, housing, environment and highly relevant area is internet of things. A lot of review articles concerning organic-inorganic hybrid nanostructure materials have been reported for the design of hybrid polymers and silicon-carbon networks (Chujo, 1996; Loy and Shea, 1995; Novak, 1993). A variety of silicates, polysiloxanes etc modified with organic groups for the improvement of mechanical properties have been investigated. Semiconductor organic–inorganic hybrids have been reported for its tuning of band gap as well as enhancement of other optical and electronic properties for versatile applications (Futscher *et al*, 2019; Chu *et al*, 2012). Kumar *et al*, (2020), have reported band gap tuning and charge transport in perylene diimide (PDI) and gallium nitride (GaN) interface of organic-inorganic hybrid nanostructure. The results revealed that the energy levels of the hybrid perfectly align and there is efficient charge transport from electron rich GaN to electron deficient PDI organic semiconductor.

Germanium is an important semiconductor element having use in both microelectronic industries and academics because of its excellent intrinsic electronic mobility ($\mu_e = 3900 cm^2 v^{-1} s^{-1}$), highest hole mobility ($\mu_h = 1900 cm^2 v^{-1} s^{-1}$), suitable band gap (0.67 eV) and high absorption coefficients at the wavelengths of interest 1.3 and 1.55 μm (Miya *et al*, 1979). Nowadays, germanium is still a comparatively rare element, however, one with great technological importance. Recently, considerable activity in the organo-germanium interaction of the monoatom and the organic functional group has emerged. The most investigated Organo-germanium compounds are the germsesquioxanes. Organic molecules and polymers have inherent advantages such as high absorption coefficients, possibility to modulate electronic properties by chemical tailoring, low manufacturing cost and easy processing in large area (Kozma and Catellami, 2013). Organic based molecules have been intensively studied as an electronic material because of their good conductivity due to presence of conjugated π-orbital and easy manipulation of their properties through substitution with functional groups such as amid or nitride (Woo *et al*. 2008). These organic-based molecules have various applications in key components of electronic and optoelectronic devices such as organic field effect transistors, organic photovoltaic and organic light-emitting diodes. In the hybrid approach there is an immense variety of adducts that can be formed between organic and inorganic species. The knowledge and understanding of this new class of organic-inorganic hybrid materials is still very much limited particularly theoretical calculation. Studying and improving these properties in Germanium-Phenyl nanocluster in the gas phase is the focus of this research.

Herein, we have intensely studied the properties of novel hybrid nine-atom germanium-phenyl $[Ge_9(C_6H_5)]$ nanostructure for electronic applications. Therefore, we report the results of the investigation of the properties of germanium-phenyl [$Ge_9(C_6H_5)$] nanostructure in the gas phase using the hybrid DFT/CAM-B3LYP functional in conjunction with Lanl2dz basis set. The nine-atom germanium-phenyl$[Ge_9(C_6H_5)]$ nanostructure is a hybrid organic-inorganic material that we hope will possess interesting optoelectronic features. Little is known about ***ab initio*** DFT structure parameter calculations of neutral nine-atom germanium-phenyl nanocluster.

METHODOLOGY

DFT using the CAM-B3LYP functional and ***ab initio*** molecular orbital theory calculations were carried out to investigate the nuclear magnetic resonance (NMR) properties and natural bond orbital (NBO) analysis of germanium-phenyl [$Ge_9(C_6H_5)$] nanostructure. The PES scan was performed to predict the most stable molecular structure of the nanostructure using B3LYP/CEP-31g basis set. The most stable molecular structure was optimized at DFT/ MP2 and DFT/B3LYP methods with Lanl2dz basis set using Gaussian 09 program (Frisch *et al*, 2009) in the framework of unrestricted formalism. Harmonic vibrational frequencies were computed at the same level of theory to ascertain the existence of true minimum at the potential surface visualized via gauss-view 5.0.8 program (Frisch *et al*, 2009) in order to characterize the structure. The long-range corrected functional CAM-B3LYP was utilized to calculate within the framework the properties of germanium-phenyl [$Ge_9(C_6H_5)$] nanocluster. GaussSum 3.0 (O¹Boyle *et al*, 2008) was used to determine the density of state (DOS) spectrum with Full Width at Half-Maximum (FWHM) of 0.3 eV of the nanostructure. The energy convergence is achieved in the order of 10^{-5} eV in the current work. Furthermore, nuclear magnetic resonance (NMR) properties were calculated by invoking the most popular Gauge-Independent Atomic Orbitals(GIAO) method as implemented in Gaussian 09 package at B3LYP/6-311+G(2d,p) level of theory. The ^{1}H and ^{13}C NMR chemical shifts have been calculated by using the GIAO approach at the same level of theory.

The NMR chemical shift δ is obtained by subtracting the calculated chemical shielding tensor σ of [$Ge_9(C_6H_5)$] nanostructure from the calculated shielding tensor of a reference compound (usually tetramethyl silane TMS or TMGe): (expressed in ppm)

$$\delta = \sigma_{ref} - \sigma_{iso} \qquad (1)$$

where σ_{ref} is the Calculated shielding tensor of the reference compound(TMS for ^{1}H, ^{13}C , ^{29}Si and ^{73}Ge NMR respectively, σ_{iso} is the isotropic shielding constant defined as

$$\vec{\sigma}_{iso} = \frac{1}{3}\left(\sigma_{xx} + \sigma_{yy} + \sigma_{zz}\right) \qquad (2)$$

Also, the coupling constant between nuclei separated by 3 bonds ^{3}J varies with the dihedral angle between the bonds according to the Karplus equation (Karplus, 1959),

$$^{3}J = A + B\cos\phi + C\cos\phi, \qquad (3)$$

where A, B, C are constants coefficients with values 7,-1 and 5 respectively.

The natural bond orbital analysis has been performed using NBO 3.1 program as implemented in Gaussian 09W software package at the DFT/CAM-B3LYP/Lanl2dz level of theory. NBO analysis provides an efficient method for studying intra- and intermolecular

bonding and interaction among bonds and also provides the basis for investigating charge transfer or conjugative interaction in molecular systems (Sibel, 2017). The computation of the second order perturbation of the interaction energy of the optimized molecular structure of germanium-phenyl [$Ge_9(C_6H_5)$] nanocluster was carried out using NBO analysis. This second-order Fock matrix was used to evaluate the donor-acceptor interaction in the natural bond orbital basis. For each donor (i) and acceptor (j), the stabilization energy E_2 associated with the delocalization $i \rightarrow j$ is estimated as: (Rahmawati *et al*, 2018)

$$E_2 = \Delta E_{ij} = q_i \frac{\left[F_{ij}\right]^2}{E_j - E_i} \qquad (4)$$

where $q_i \rightarrow$donor orbital occupancy, E_i, $E_j \rightarrow$diagonal elements and $F_{ij} \rightarrow$the off diagonal NBO Fock matrix element.

RESULTS AND DISCUSSION

Natural Bond Orbital Analysis for [$Ge_9(C_6H_5)$] nanocluster

In NBO analysis, large stabilization energy values E_2 indicate intensive interaction between electron-donors and electron-acceptors and to a greater extend the conjugation of the whole system. The results of NBO analysis of germanium-phenyl [$Ge_9(C_6H_5)$] nanostructure are shown in Table 1. The charge density map of HOMO and LUMO for novel germanium-phenyl [$Ge_9(C_6H_5)$] nanostructure is also shown in Figure 1. The studied optimized molecular structure of germanium-phenyl [$Ge_9(C_6H_5)$] nanostructure is shown in Figure 2.

As observed from Table 1, the intramolecular hyperconjugative interactions of $BD(1)(Ge_4 - Ge_6) \rightarrow LP^*(1)(Ge_8)$, $BD(1)(Ge_5 - Ge_6) \rightarrow LP^*(1)Ge_7$, $BD(1)(Ge_1 - Ge_6) \rightarrow LP^*(2)Ge_7$, $BD(1)(Ge_4 - Ge_{20}) \rightarrow LP^*(1)Ge_3$ 4 $BD(1)(Ge_5 - Ge_{20}) \rightarrow LP^*(2)Ge_2$, $BD(2)(C_{12} - C_{16}) \rightarrow BD^*(2)(C_9 - C_{10})$, $BD(2)(C_{11} - C_{14}) \rightarrow BD^*(2)(C_{12} - C_{16})$, $BD(2)(C_9 - C_{10}) \rightarrow BD^*(2)(C_{11} - C_{14})$, $BD(1)(Ge_1 - Ge_2) \rightarrow LP^*(2)Ge_7$, $BD(1)(Ge_1 - Ge_3) \rightarrow LP^*(2)Ge_8$, $BD(1)(Ge_4 - Ge_8) \rightarrow LP^*(1)Ge_3$ and $BD(1)(Ge_5 - Ge_7) \rightarrow LP^*(2)Ge_2$ have highest stabilization energy and electron density values of 81.36[E_D= 0.70369e],80.74[E_D=0.70430e],65.63[E_D=0.74783e],31.26[E_D=0.85129e],30.85 [E_D=0.85303e],17.81[E_D=0.82307e],16.14[E_D=0.82620e],15.38[E_D=0.82620e],14.39[E_D=0.720369e] ,14.27[E_D=0.72157e],13.49[E_D=0.69159e] and 13.34[E_D=0.69220e] Kcal/mol at CAM-B3LYP level respectively.

These greatest stabilization energies are associated to electron delocalization(E_D) between the donor-acceptor interactions. The magnitude of charges transferred from the lone pair to the antibonding increases the electron density in the respective bond. From our results, NBO analysis clearly explain the evidence of the formation of a weak H-bonded interaction between the LP(1)Ge_6 and LP*(2)Ge_7, BD(1)Ge_1-Ge_2 and LP*(2)Ge_3, LP(1)Ge_2 and LP*(1)Ge_{20}, LP(1)Ge_7 and BD*(1)Ge_4-Ge_6, LP(1)Ge_8 and BD*(1)Ge_5-Ge_6, BD(1)Ge_1-Ge_3 and BD*(1)Ge_3-Ge_8 respectively. Furthermore the energetic contribution of LP(1)$Ge_6 \rightarrow$LP*(2)Ge_7[9.14 Kcal/mol],BD(1)(Ge_1-Ge_2) $\rightarrow$LP*(2)Ge_3[8.42,Kcal/mol], LP(1)$Ge_2 \rightarrow$LP*(1)Ge_{20}[7.35Kcal/mol],LP(1)$Ge_7 \rightarrow$BD*(1)(Ge_4-Ge_6)[5.21Kcal/mol], LP(1)$Ge_8 \rightarrow$BD*(1)(Ge_5-Ge_6)[5.20 Kcal/mol] and BD(1)(Ge_1-Ge_3) $\rightarrow$ BD*(1)(Ge_3-Ge_8)[2.37 Kcal/mol] of hyperconjugation interaction is weak, these E_2 stabilization values are

chemically significant and can be used as a measure of the intramolecular delocalization. These weak occupancies of the valence antibonding signal irreducible departures from an idealized Lewis picture. According to our results, the intramolecular charge transfer $\pi \rightarrow \pi^*$, $n \rightarrow \pi^*$, $n \rightarrow \sigma^*$ occurs in germanium-phenyl [$Ge_9(C_6H_5)$] nanostructure

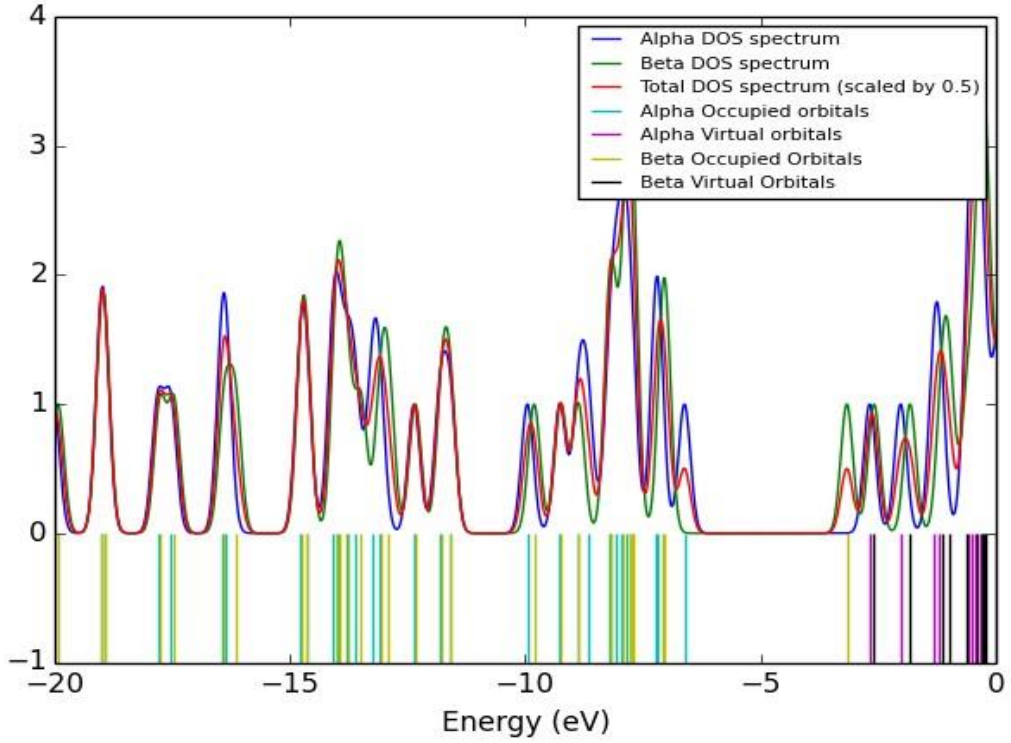

Figure 1: HOMO, LUMO and Density of State of [$Ge_9(C_6H_5)$] nanocluster.

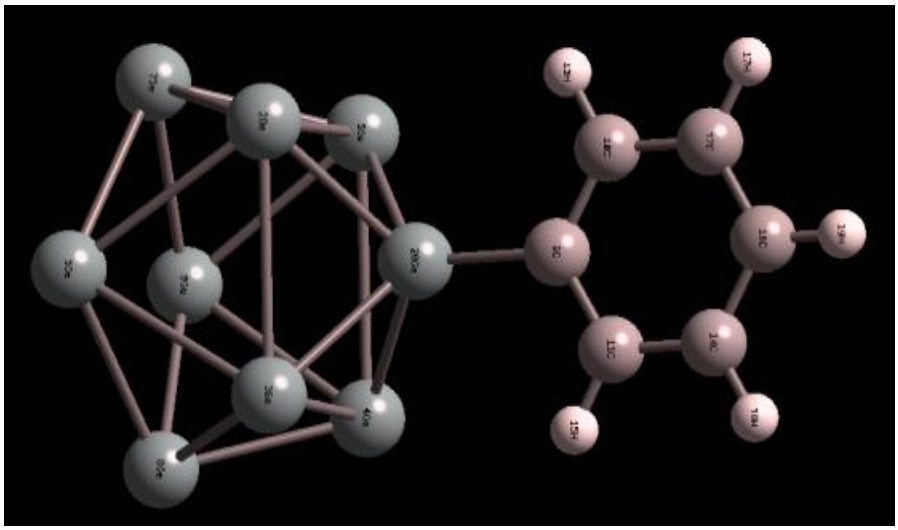

Figure 2: Molecular Structure of [$Ge_9(C_6H_5)$] nanocluster(Njapba and Galadanci, 2021).

Table 1: Second –order perturbation theory analysis of Fock Matrix in NBO basis for germanium-phenyl [$Ge_9(C_6H_5)$] nanostructure.

Donor (i)	ED(e)	Energy(i) a.u	Acceptor (j)	ED(e)	Energy(j) a.u	E2 Kcal/mol	Ei - Ej (a.u)	F(i,j) a.u
BD(1)Ge1-Ge2	0.72096	-0.27547	LP*(2)Ge3	0.31467	-0.06186	8.42	0.21	0.055
BD(1)Ge1-Ge2	0.72096	-0.27547	LP*(2)Ge7	0.34850	-0.07503	14.39	0.20	0.070
BD(1)Ge1-Ge3	0.72157	-0.27578	LP*(2)Ge8	0.34812	-0.07507	14.27	0.20	0.070
BD(1)Ge1-Ge3	0.72157	-0.27578	BD*(1)Ge3-Ge8	0.04290	-0.07305	2.37	0.35	0.041
BD(1)Ge1-Ge6	0.74783	-0.28002	LP*(2)Ge7	0.34850	-0.07503	65.63	0.20	0.154
BD(1)Ge4-Ge6	0.70369	-0.23847	LP*(1)Ge8	0.34812	-0.07507	81.36	0.16	0.149
BD(1)Ge4-Ge8	0.69220	-0.29730	LP*(2)Ge3	0.31467	-0.61861	13.34	0.24	0.071
BD(1)Ge4-Ge20	0.85129	-0.39342	LP*(1)Ge3	0.92304	-0.41190	31.26	0.33	0.141
BD(1)Ge5-Ge6	0.70432	-0.23872	LP*(1)Ge7	0.34850	-0.07503	80.74	0.16	0.149
BD(1)Ge5-Ge20	0.85303	-0.39380	LP*(1)Ge2	0.31443	-0.06352	30.85	0.33	0.140
BD(2)C9-C10	0.83495	-0.30776	BD*(2)C11-C14	0.15653	-0.06429	15.38	0.37	0.096
BD(2)C11-C14	0.82620	-0.30080	BD*(2)C12-C16	0.16088	-0.06383	16.14	0.36	0.097
BD(2)C12-C16	0.82307	-0.29937	BD*(2)C9-C10	0.18441	0.05174	17.81	0.35	0.100
LP(1)Ge2	0.96042	-0.41567	LP*(1)Ge20	0.45274	-0.12983	7.35	0.29	0.076
LP(1)Ge6	0.95761	-0.42088	LP*(2)Ge7	0.34850	-0.07503	9.14	0.35	0.085
LP(1)Ge7	0.93968	-0.40585	BD*(1)Ge4-Ge6	0.05933	-0.00336	5.21	0.40	0.058
LP(1)Ge8	0.93965	-0.40580	BD*(1)Ge5-Ge6	0.05945	-0.00387	5.20	0.40	0.058
BD(1)Ge5-Ge7	0.69159	-0.29740	LP*(2)Ge2	0.31443	-0.06352	13.49	0.23	0.021

NMR Analysis

The NMR parameters obtained here are the results of DFT calculations using Gaussian 09 software package and invoking the guage-independent atomic orbitals (GIAO) method. The molecular model was calculated in the gas phase. The B3LYP/6-311+G(2d,p) functional was used for structure optimization as well as for ^{1}H, ^{13}C and ^{73}Ge NMR shielding constants calculations. The isotropic chemical shielding for ^{1}H, ^{13}C and ^{73}Ge complexes were referenced to standard compound tetramethysilane (TMS). We present in Table 2 and 3 and Figure 3 and Figure 4, the results of chemical shift and spin-spin coupling in germanium-phenyl [$Ge_9(C_6H_5)$] nanostructure calculations from First principles.

Chemical Shift (δ)

Table 2 is the ^{1}H NMR spectral data of germanium-phenyl nanostructure. It is observed that there are five hydrogen atoms of the [$Ge_9(C_6H_5)$] nanostructure with shielding values all being positive i.e., there is a shielding effect. All these protons display quite close calculated chemical shift (δ ppm) values with approximate difference of about 0.4 ppm indicating similarities in conformation and intermolecular interactions. Wang *et al*, (2001) reported that the range of ^{1}H change is only within 2-3 ppm but predicted values must be accurate to about 0.1ppm to be valuable as markers conformational state. Many authors have calculated proton shielding for very small molecules to be ± 0.1 ppm absolute accuracy (Sundholm *et al*, 1996; Chesnut, 1997; Sauer *et al*, 1997). Chemical shifts in the region $6.5-8.0$ ppm in ^{1}H NMR spectrum usually appeared due to NMR of aromatic protons indicating the presence of hydrogen in the complex (Levitt, 2008; Macomber, 1998). Soderberg (2016) have reported that protons in organic compounds have chemical shift values between 0 and 10 ppm relative to TMS, although values below 0 ppm and up to 12 ppm and above are occasionally observed.

For [$Ge_9(C_6H_5)$] nanostructure, the ^1H NMR chemical shift as found in Figure 3 increases to the left with positive values of 6.20, 6.52, 6.61, 6.65 and 6.95 ppm respectively, denoting a downfield i.e. a high frequency. This aromatic hydrogen is deshielded as a direct consequence of the magnetic anisotropic of the $\pi-$electrons. Remember the resonance structure of the aromatic compound Benzene. In an applied magnetic field, the $\pi-$electrons begin to circulate along the resonance forming what is known as ring current that generates an analogous induced field. Above and below the centre of the ring, the induced field is opposed to the external field giving rise to shielding effect on the nuclei. However, outside the periphery of the ring where aromatic hydrogen is located, the induced field is aligned with the external field causing a deshielding of the hydrogen nuclei.

Table 2: Calculated Shielding Constant[$\sigma=$ppm] and Chemical Shift[$\delta=$ppm] for isolated ground state [$Ge_9(C_6H_5)$] nanostructure with B3LYP/6-311+G(2d,p) functional.

Number of ^{73}Ge	σ (ppm)	$\delta=\sigma_{ref}-\sigma$ (ppm)	Number of ^1H	σ (ppm)	$\delta=\sigma_{ref}-\sigma$ (ppm)	Number of ^{13}C	σ (ppm)	$\delta=\sigma_{ref}-\sigma$ (ppm)
1	2225.84	-895.84	13	25.24	6.65	9	88.49	93.98
2	1960.83	-630.83	15	25.68	6.20	10	25.50	156.97
3	2382.52	-1052.52	17	25.27	6.61	11	28.76	153.71
4	1946.21	-616.21	18	25.36	6.52	12	49.60	132.86
5	2413.02	-1083.02	19	24.93	6.95	14	49.77	132.69
6	2149.79	-819.79				16	42.79	139.67
7	2190.36	-860.36						
8	2234.59	-904.59						
20	2647.49	-1317.49						

^{73}Ge **($GeMe_4$),** $\sigma_{ref}=1330$ppm, ^{13}C **($SiMe_4$),** $\sigma_{ref}=182.47$ppm, ^1H **($SiMe_4$),** $\sigma_{ref}=$ 31.88ppm.

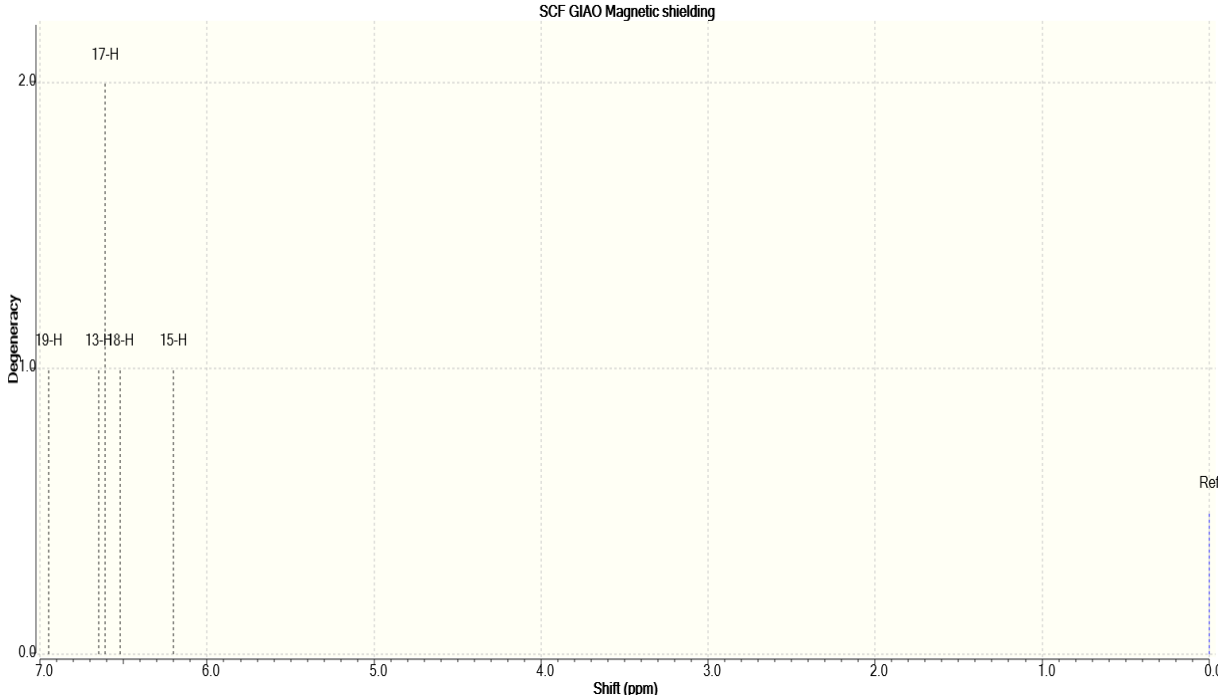

Figure 3: ^1H **NMR** Chemical Shift of [$Ge_9(C_6H_5)$]

As observed from Figure 3, ^{1}H NMR spectra contain proton signals that split into a number of peaks, though there are no subpeaks. The splitting patterns and relative intensities of the peaks are consistent with the solid state structure. The peaks attributable to [$Ge_9(C_6H_5)$] nanostructure are clustered to essentially give identical patterns for all five protons with their chemical shift being in the range $6.202-6.947$ ppm. All ^{1}H NMR chemical shifts have a degeneracy of one; with H19 having the highest chemical shift $\delta = 6.95$ ppm while H17 has a degeneracy of two and chemical shift $\delta = 6.61$ ppm. This splitting behavior is actually useful because it provides more information about the sample cluster. Furthermore, the ^{1}H NMR chemical shifts look identical due to similar chemical environment and similar atomic neighbors.

The ^{13}C NMR spectral data are also given in Table 2. The chemical shift of ^{13}C NMR nuclei are measured from the reference compound tetramethysilane (TMS) having a value of σ_{ref} = 182.47ppm (^{13}C **(**$SiMe_4$**)**). Figure 4 shows the ^{13}C NMR spectra.

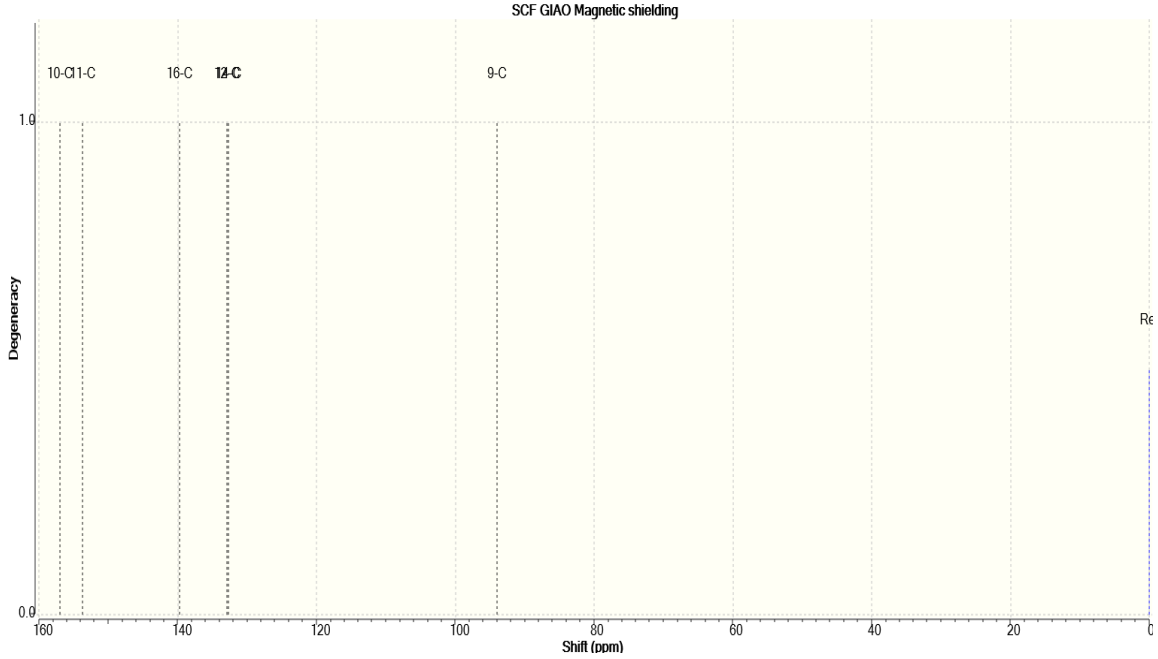

Figure 4: ^{13}C NMR chemical shift spectra calculated at B3LYP/6-311+G(2d,p) level

Again, from Table 2, all the chemical shielding constants $\sigma(ppm)$, are all positive and clustered far to the left, implying increasing magnetic shielding. It can be observed that the chemical shift of the nine-atom germanium-phenyl nanostructure is in the range 93.99 to 156.97 ppm. The chemical shifts differ from each other; it is downfield and computed on the most symmetrical B3LYP geometries with gradual increase. Notice that the aromatic carbons appear slightly downfield of the Vinyl carbons just as aromatic hydrogen appeared downfield. Typical chemical shifts of ^{13}C NMR range normally from $0-250$ ppm (Oturak *et al*, 2015; Gerothanassis *et al*, 2002). These shifts observed in a nucleus are influenced by the state of hybridization such as sp^3, sp^2 and sp. Our nanostructure exhibits two states of hybridization, sp^2 and sp respectively. Between 132.69 to 156.97 ppm, our calculated results fall in the range of sp^2 hybridization that ranged from 120 to 240 ppm, while 93.94ppm falls below 100ppm and that is sp hybridization. Banwell (1994) observed that ^{13}C NMR chemical shifts have wide range thus its spectra usually contains separate resonances for each chemically shifted nucleus in the molecule (i.e. very little overlap of resonance occurs).

However, we observed an overlap between C_{12} and C_{14} with chemical shift values of 132.86 ppm and 132.69 ppm respectively. ^{13}C NMR is very useful in structural characterization since it is less sensitive to such factors as temperature solvent and pH.

Also listed in Table 2 is the ^{73}Ge NMR data. ^{73}Ge NMR possesses only one active magnetic isotope with spin $I = \frac{9}{2}$ and relatively large quadrupole moment of about -196mb (Weinert, 2012; Pyykko, 2008). The sensitivity with respect to ^{1}H at natural abundance and constant field is 1.08×10^{-4}. The magnetic shielding $\sigma(ppm)$ was computed using GIAO approach as implemented in Gaussian 09 program. The magnetic shielding resonance lines observed for ^{73}Ge NMR spectra are broad, positive and increasing far to the right. For germanium, the quadrupole relaxation moment dominates, dipole-dipole relaxation and nuclear overhauser effects are not important thus, the unsymmetrical ^{73}Ge will give rise to an inherently broad line resonance as viewed in germanium-phenyl [$Ge_9(C_6H_5)$] nanostructure. The positive nature of the isotropic chemical shielding of ^{73}Ge NMR values, means the germanium nucleus is well shielded. The ^{73}Ge NMR chemical shifts were calculated relative to tetramethylgermane ($GeMe_4$) that is a reference compound with value $\sigma_{ref} = 1330$ppm. The chemical shift of nine-atom germanium-phenyl [$Ge_9(C_6H_5)$] nanostructure consist of nine resonance lines in the range -616.21 to -1317.49 ppm. It is observed that the lines are all negative, sharp, also far to the right and signifying increased shielding of the Ge nucleus with resonance shifted upfield i.e. low frequency. The upfield shift arises from electron-rich electropositive Ge and the change in hybridization of the Vinyl carbons towards less s-character (i.e. more sp^3 like). Many authors have reported that most germanium compounds calculated NMR chemical shift relative to the reference compound $GeMe_4$ being negative and also upfield (Amadoruge *et al*, 2009; Liepins *et al*, 1988; Weinert, 2012). Ge_{20} in [$Ge_9(C_6H_5)$] nanostructure is the central atom bonded to more than four other atoms of germanium with carbon inclusive, has a chemical shift of about -1317.49 ppm. The observed resonance for this central atom means it is more shielded than others. Weinert, (2012) compared the chemical shift of two compounds, phenyl-germanium complex [$Pr_3^i GeGePh_3$] and alkyl-germanium [$Bu_3^n GeGePh_3$] complex with observed resonances of -65ppm and -56ppm respectively. These results indicate that the phenyl-germanium complex is consistently upfield. The ^{73}Ge NMR chemical shift for Ge compounds particularly GeI_4 exhibit a single resonance at -1171 ppm (Weinert, 2012). Amadoruge *et al*, (2009) reported resonance peaks for singly bonded oligogermane compounds; $Me_3GeGeMe_3$, $Ph_3GeGePh_3$ and $(Ph_3Ge)_3GeH$ with observed chemical shift of -59, -67 and -314 ppm that were calculated relative to $GeMe_4$. The maximum peak of -314ppm corresponds to the central germanium atom in $(Ph_3Ge)_3GeH$. They also observed that germanium as the central atom having only one attached Ge atom result in resonances appearing in the range -30 to -65 ppm, while that having two or three bonded Ge atoms exhibit resonances in the respective range of -100 to -120 ppm or -195 to -210 ppm.

Spin-Spin Coupling Constant (or J-Coupling)

The three-bond $^{3}J-$coupling constant is dependent on the dihedral angle between the bonds. The $^{3}J-$coupling constant as function of dihedral angle given by equation (3) has been computed. The results are shown in Table 3. The plot is given by Figure 5.

Table 3: Calculated $^3J-$ Coupling for Different Dihedral angles.

S/N	Dihedral Angles	$^3J-$ coupling	
1	Ge2-Ge3- Ge4- Ge5 =0.0006	$^3J(Ge,Ge)$	11
2	Ge1- Ge2- Ge20-Ge4 =09.652	$^3J(Ge,Ge)$	10.73
3	Ge1- Ge3- Ge20- Ge4 =15.44	$^3J(Ge,Ge)$	10.33
4	Ge3- Ge1- Ge7- Ge5 = 19.29	$^3J(Ge,Ge)$	9.96
5	Ge6- Ge4- Ge20- Ge2 = 27.819	$^3J(Ge,Ge)$	8.94
6	Ge20- Ge2- Ge7- Ge6 = 35.215	$^3J(Ge,Ge)$	7.86
7	Ge1- Ge3- Ge4- Ge5 = 58.539	$^3J(Ge,Ge)$	4.20
8	Ge6- Ge1- Ge3- Ge20 = 48.375	$^3J(Ge,Ge)$	9.66
9	C11- C9- C10- C12 = 0.201	$^3J(C,C)$	10.99
10	C11- C9- C10- C13 =179.887	$^3J(C,C)$	12.99
11	C9- C11- C14- C16 =0.015	$^3J(C,C)$	10.99
12	H17- C12- C16- H19 =0.16	$^3J(H,H)$	10.99
13	H17- C12- C16- H19 =0.16	$^3J(C,H)$	10.99

Table 3 shows the calculated values of $H-H, C-H, C-C$ and $Ge-Ge$ $^3J-$coupling constants. Our discussion is focused more on $^3J(H-H)$, $^3J(C-H)$, $^3J(C-C)$ coupling constants since most accurate calculations of spin-spin coupling constant have been computed for hydrogen atoms and also for easy comparison with [$Ge_9(C_6H_5)$] nanostructure. Plot of $^3J-$coupling constant against dihedral angles is given in Figure 5**.** From the Table, it can be found that all the coupling constant is positive. The positive nature of these values reflects the strong interaction between the coupling nuclei and the arrangement of the atoms within the nanostructure. The theoretically calculated values of the coupling constant in the gas phase are $^3J(H-H)=10.99$ Hz, $^3J(C-H)=10.99$ Hz, and $^3J(C-C)=12.99$ Hz respectively. The experimentally calculated values are $^3J(H-H)=11.0$ Hz, $^3J(C-H)=7.7$ Hz and $^3J(C-C)=10.12$ Hz respectively (Fukui, 1999). Clearly, the theoretically calculated coupling constant of $^3J(C-H)$ is bigger than the experimental value with a difference of about 3.29 Hz, similarly the difference of $^3J(C-C)$ coupling constant is about 2.87Hz. Helgaker *et al*, (1999) reported an experimental calculated $^3J-$coupling constant of $^3J(C-H)$ with difference in the range from 2-3Hz. This difference arises due to electron delocalization between the carbon-hydrogen bonds. Furthermore, the variation in the magnitude of the three-bond couplings can be related to the position of the coupling proton. Fukui *et al*, (1995) analyzing the angular dependence of the coupling constant $^3J(H-H)$, on the dihedral angle reported that the calculated values were underestimated by as much as 1.5 to 4.5 Hz compared to experimental values. They attributed such difference to geometric effects or lack of higher order correlation in the calculations. Biedrzycka *et al*, (2006), presented quantum mechanical DFT calculations of aromatic carbon-carbon spin-spin coupling in Benzene, nitrobenzene, p-substituted nitrosobenzene and O-nitrosotoluene. Their results revealed that the $^3J(C-C)$ coupling constant was obtained over a broad range from 8 to 10 Hz in Benzene and nitrosobenzene. Our theoretically calculated values fall in this range.

From Figure 5, the proton-proton $^{3}J(H-H)$, coupling constant bell-shaped curve reaches maximum values at 0^{0} and 179.88^{0} (i.e. $^{3}J=11$Hz and $^{3}J=12.99$Hz respectively) and its minimum value at 90^{0} (i.e. $^{3}J=4.2$Hz). This is due to stereoelectronic interaction between the two vicinal molecular orbitals, is at maximum when the orbitals are parallel (i.e. dihedral angles of 0^{0} and 179.88^{0}) and decreases almost to zero when the orbitals are perpendicular (dihedral angle of 90^{0}). There is the presence of $\pi-$conjugation in the nanostructure that has some important consequence, the cis (0^{0}) or trans (179.88^{0}). Because of the presence of $\pi-$ conjugation, more electron communicating spins information between the nuclei and $^{3}J(H-H)$, is greater than in the case of all single bonds. The proton-proton $^{3}J(H-H)$, coupling constant values for cis across a double bond are typically 10-12 Hz, while for a trans its values are within the range 16-18Hz (Macomber, 1998).

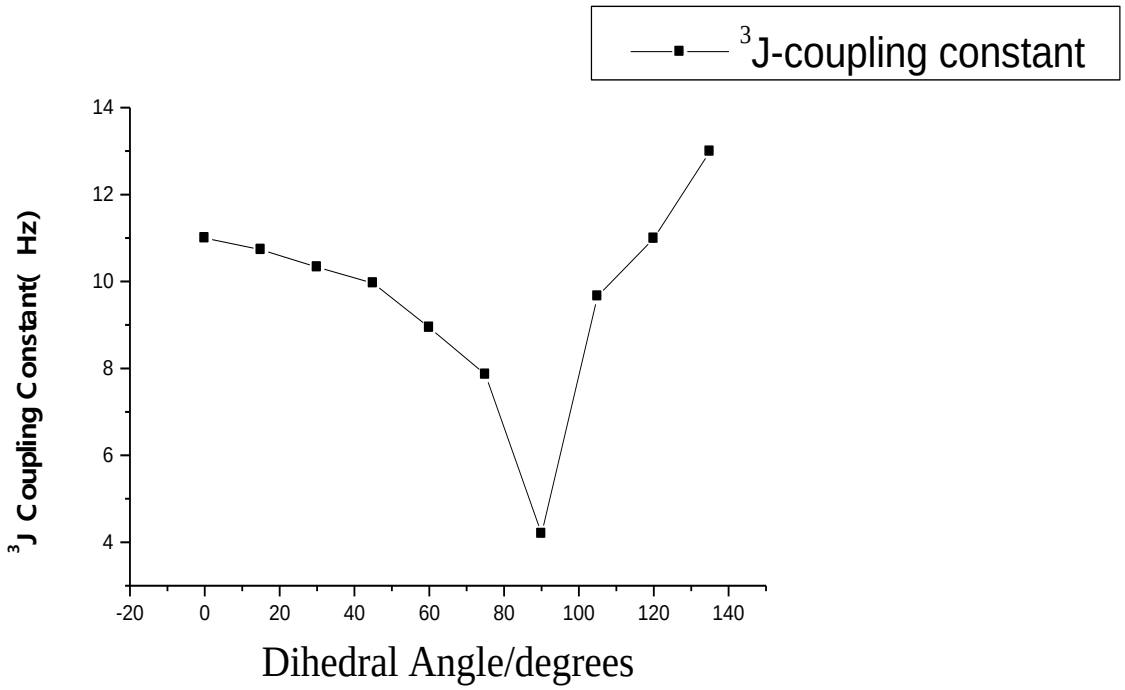

Figure 5: Plot of $^{3}J-$ coupling constant as Function of Dihedral Angle

CONCLUSION

The nuclear magnetic resonance properties and natural bond analysis of nine-atom germanium-phenyl [$Ge_9(C_6H_5)$] nanostructure in the gas phase were investigated with DFT/B3LYP and CAM-B3LYP with Lanl2dz and 6-311+G(2d,p) basis sets as implemented in Gaussian 09 software package. ^{1}H , ^{13}C , ^{73}Ge NMR chemical shift and Spin-Spin coupling constant(^{3}J -coupling) of [$Ge_9(C_6H_5)$] nanostructure were calculated using Gauge-including atomic orbitals(GIAO) approach and results compared with experimental data. ^{1}H NMR chemical shifts are in the range $6.202-6.947$ ppm, ^{13}C NMR chemical shift in the nine-atom germanium-phenyl nanostructure are in the range 93.99 to 156.97 ppm while ^{73}Ge NMR chemical shift of nine-atom germanium-phenyl [$Ge_9(C_6H_5)$] nanostructure are in the range -616.21 to -1317.49 ppm are in good agreement with experimental results. The theoretically calculated values of the coupling constant in the gas phase are $^{3}J(H-H)=10.99$ Hz,

$^3J(C-H) = 10.99$ Hz, and $^3J(C-C) = 12.99$ Hz respectively and are observed to be bigger than the experimental value with a difference of about 3.29 Hz. In germanium-phenyl [$Ge_9(C_6H_5)$] nanostructure, NBO analysis reveals that a strong intramolecular hyperconjugative interaction of electrons with large energy contribution from $BD(1)(Ge_4 - Ge_6) \rightarrow LP^*(1)Ge_8$ have energy value of 81.36 Kcal/mol.

REFERENCES

Abbas H., Mohd S., and Alfaify S. (2019). Density Functional Study of Spectroscopy, Electronic Structure, Linear and Nonlinear Optical Properties of L-proline Lithium Chloride and L-proline Lithium Bromide Monohydrate for Laser Application. *Arabian Journal of Chemistry. Vol. 12, no.8, pp2336-2346*.

Amadoruge M. L., Yoder C. H., Conneywerdy J. H., Heroux K., Arnold L. R., and Weinert C.S. (2009). ^{73}Ge NMR Spectral Investigations of Singly Bonded Oligogermane. *Organometallic, 28(10), pp3067-3073. American Chemical Society*.

Banwell C. N. (1994). Fundamentals of Molecular Spectroscopy (4th Ed.). New York: Mc Graw Hill.

Biedrzycka Z., Kamienska T. K., and Witanowski M. (2006). Indirect Carbon-Carbon Spin-Spin Coupling in Nitrosobenzene and Benzene. Experimental and Theoretical, *Polish Journal of Chemistry, Vol. 80, no.7, pp1195-1207*

Carraro M. and Gross S. (2014). Modified Transition Metal Oxoclusters or Polyoxometalates into Polymers for Functional Applications. A Review. *Materials, 7 pp 3956-3989*

Chesnut D. B. (1997). Ab initio NMR Chemical Shielding in the Neutral and Charged 7-Phosphabicyclo [2.2.1] Heptanes, -Heptene, and -Heptadiene Systems: The largest Predicted Downfield Shift for a Conventional Organophosphorus Molecule. *Chemical Physics, 24, 73, pp133–141*.

Chu, X. Guan M., Li L., Zhang Y., Zhang F., Li Y.,Zhu Z., Wang B. and Zeng Y.(2012). Improved Efficiency of Organic/Inorganic Hybrid Near-Infrared Light Upconverter by Device Optimization. *ACS Applied Materials and Interfaces 4(* **9)**, pp4976–4980. DOI: 10.1021/am301340p

Chujo Y.(1996). Organic-Inorganic Hybrid Material. *Current Chemistry Ltd*, 1; pp 806-811.

Frisch, M. J., Trucks, G.W., Schlegel, H. B., Scuseria, G. E., Robb, M.A., Cheeseman, J. R., Scalmani, G., Barone, V., Mennucci, B., Petersson, G.A., Nakatsuji, H., Caricato, M., Li, X., Hratchian, H. P., Izmaylov, A. F., Bloino, J., Zheng, G., Sonnenberg, J. L., Hada, M., Ehara, M., Toyota, K., Fukuda, R., Hasegawa, J., Ishida, M., Nakajima, T., Honda, Y., Kitao, O., Nakai, H., Vreven, T., Montgomery, J. A., Jr., Peralta, J. E., Ogliaro, F., Bearpark, M., Heyd, J. J., Brothers, E., Kudin, K. N., Staroverov, V. N., Kobayashi, R., Normand, J., Raghavachari, K., Rendell, A., Burant, J. C., Iyengar, S. S., Tomasi, J., Cossi, M., Rega, N., Millam, J. M., Klene, M., Knox, J. E., Cross, J. B., Bakken, V., Adamo, C., Jaramillo, J., Gomperts, R., Stratmann, R. E., Yazyev, O., Austin, A. J., Cammi, R., Pomelli, C., Ochterski, J. W., Martin, R. L., Morokuma, K., Zakrzewski, V. G., Voth, G. A., Salvador, P., Dannenberg, J. J., Dapprich, S., Daniels, A. D., Farkas, Ö., Foresman, JB., Ortiz, JV., Cioslowski, J. and Fox, D.J. **2009. Gaussian 09, Revision E.01, Gaussian, Inc., Wallingford CT.**

Fukui H.(1999). Theory and Calculation of Nuclear Spin-Spin Coupling Constants. *Progress in Nuclear Magnetic Resonance Spectroscopy, 35, pp267-294, Elsevier.*

Fukui H., Inomata H., Baba T., Miura K., and Matsuda H. (1995). Calculation of Nuclear Spin-Spin Couplings VIII. Vicinal Proton-Proton Coupling Constants in Ethane. *Journal Chemical Physics, Vol. 103, no. 15, pp6597-6600.*

Futscher, M. H. Thorsten S., Johannes F., Maryline R., Ezzeldin M., Marco V. N., Muller-Buschbaum P., and Norbert K. (2019).Electronic Properties of Hybrid Organic/Inorganic Semiconductor PN-Junctions. *Journal of Physics*:*Condense Matter* 31**,** 064002. DOI: 10.1088/1361-648X.

Gerothanassis I. P., Troganis A., Exarchou V. and Barbarossa K. (2002). Nuclear Magnetic Resonance Spectroscopy: Basic Principles and Phenomena and their Applications to Chemistry, Biology and Medicine. Chemistry Education: *Research and Practice in Europe, Vol. 3, no. 2 pp229-252.*

Helgaker J., Jaszunski M., and Ruud K. (1999). Ab Initio Methods for the Calculation of NMR Shielding and Indirect Spin-Spin Coupling Constants. *Chemical Review, Vol. 99, no.1, pp293-352.*

Kagan C.R., Mitzi D.B., and Dimitrakopoulos C.D (1999). Organic-inorganic Hybrid Materials as Semiconducting Channels in Thin-Film Field Effect Transistors. *Science, Vol. 286. pp945-947*

Karplus M. (1959). Contact Electron-Spin Coupling of Nuclear Magnetic Moments. *Journal Chemical Physics. Vol. 30, pp11-15*

Kozma E. and Catellami M.(2013). Perylene Diimide Based Materials for a Organic Solar Cells. *Dyes and Pigments*, 98, pp160-179 Elsevier

Kumar R., Sunil S.K., Mahesh K., Muthusamy S. K., Govind G., Kavindra K., and Pramod K.(2020). Flexible Perylene Diimide/GaN Organic–Inorganic Hybrid System with Exciting Optical and Interfacial Properties. *Scientific Report*, Vol. 10, pp1-21.

Levitt M. H. (2008). Spin Dynamics, Basics of Nuclear Magnetic Resonance, 2nd Edition. John Wiley & Sons Ltd.

Liepins E., Zicmanc I., and Lukevics E. (1988). ^{73}Ge NMR Spectroscopic Studies of Organogermanium Compounds. *Journal of Organometallics Chemistry, 341, pp315-333*

Loy D. A. and Shea K. J. (1995). Bridged Polysilsesquioxanes Highly Porous Hybrid Organic-Inorganic Materials. *Chemical Review.* **95**, pp1431–1442.

Macomber R. S. (1998). A Complete Introduction to Modern NMR Spectroscopy. John Wiley & Sons Inc.

Njapba A. S. and Galadanci G.S.M. (2021). Electronic Structure, Optical and Thermodynamic Properties of Germanium-Phenyl Nanocluster in the Gas-phase: A DFT Study. *International Journal of Engineering and Applied Science*.Vol.2, Number 1, pp1-31.

Novak, B. M. (1993). Hybrid Nanocomposite Materials-between Inorganic Glasses and Organic Polymers. *Advanced Material* **5**, pp422–433.

O'Boyle N. M., Tenderholt A. L., and Langner K. M."Cclib (2008): A Library for Package-Independent Computational Chemistry Algorithms," *Journal of Computational Chemistry*, Vol. 29, no. 5, pp839–845.

Oturak H., Kimyturk N. K., and Sahn G. (2015). Structure and Vibrational Studies of 1-(1H-Benzoimidazol-2-yl) Ethanol, Using DFT Method. *Acta Physica Polonica A. Vol. 128, no. 2B*.

Pyykko P. (2008). Year-2008 Nuclear Quadrupole Moments. *Molecular Physics, Vol. 106(16-18), pp1965-1974.*

Rahmawati S., Radiman C.L., and Muhamad A.M.(2018). Density Functional Theory and Natural Bond Analysis of Intermolecular Hydrogen Bond interaction in Phosphorylated Nata de Coco-Water. Indonesian Journal of Chemistry, 8(1), pp173-178. DOI:10.22146/ijc.25170.

Sauer S. P. A., Spirko V., Paidaraova I., and Kraimer W. P. (1997). *Chemical Physics, 214, 91.*

Sibel D. K.(2017). Investigation of theoretical calculation of 2-(1-Phenylethlideneamino) Guanidine compound: NBO,NLO, HOMO-LUMO and MEP Analysis by DFT Method. *Karaelmas Fen Muh, Derg*, 7(2) pp491-496.

Soderberg T. (2010). Organic Chemistry with a Biological Emphasis, Vol.1, Chapter 1-8.

Sundholm D., Gauss J., and Schafer A. (1996). *Journal Chemical Physics, 105, 1491.*

Wang B., Ulrich F., James F.H., and Pulay P. (2001). Accurate Prediction of Proton Chemical Shift. I. Substituted Aromatic Hydrocarbon. *Journal of Computational Chemistry, Vol. 22, no.16, pp1887-1895. John Wiley & Sons Inc.*

Weinert C. S. (2012). ^{73}Ge Nuclear Magnetic Resonance Spectroscopy of Ge Compounds. *International Scholarly Research Network, Vol. pp 1-19.*

Woo Y.K., Young C.C., and Kwang S.K. (2008). Understanding Structures and Electronic/ Spintronic Properties of Single Molecules, Nanowires, Nanotubes, and Nanoribbons towards the Design of Nanodevices. *Journal of Material Chemistry, 18, pp4510-4521*